IEEE Access
Multidisciplinary | Rapid Review | Open Access Journal

Received January 21, 2018, accepted February 16, 2018, date of publication February 21, 2018, date of current version March 12, 2018.

Digital Object Identifier 10.1109/ACCESS.2018.2808362

A Frequency Synthesizer Based Microwave Permittivity Sensor Using CMRC Structure

SHICHANG CHEN, (Member, IEEE), MENGCHU GUO, KUIWEN XU, PENG ZHAO, (Member, IEEE), LINXI DONG, AND GAOFENG WANG, (Senior Member, IEEE)
Key Laboratory of RF Circuits and Systems, Ministry of Education of China, Hangzhou Dianzi University, Hangzhou 310018, China

Corresponding author: Shichang Chen (eechensc@hdu.edu.cn)

This work was supported by the National Natural Science Foundation of China under Grant 61601160, Grant 61601163, Grant 61411136003, and Grant 61331007.

ABSTRACT In this paper, a high-sensitive microwave dielectric sensor targeted for material permittivity characterization is proposed. A reflective voltage controlled oscillator is devised by virtue of the compact microstrip resonant cell (CMRC) and embedded into a fractional-*N* phase-locked loop frequency synthesizer. The CMRC structure, covered with material under test, changes its resonating characteristics and, hence, the initial oscillating frequency. Due to the presence of the frequency synthesizer, this frequency shift is finally translated into the controlling voltage variation. In this paper, the material permittivity is extracted by measuring the voltage deviation. Several different samples with known permittivity values are tested to verify the effectiveness of the design sensing platform.

INDEX TERMS Compact microstrip resonant cell, frequency synthesizer, microwave sensor, permittivity characterization, reflective oscillator.

I. INTRODUCTION

Dielectric constant is an important feature of material in engineering. The accurate electrical knowledge of permittivity (i.e., dielectric constant) provides much valuable information about the material under test (MUT). Precise characterization of this material property can find numerous applications. Reported applications include but not limited to food quality monitoring [1], [2], biological material detection [3]–[6], blood glucose measurement [7], [8], humidity and gas concentration sensing [9]–[11], as well as liquid composition analysis [12]–[14]. The microwave approach, thanks to its non-invasive and nondestructive feature, gains great popularity in recent years. By exciting the material with a high-frequency signal and recording the transmission or reflection response, the microwave method may achieve high accuracy in a wide frequency band.

In view of different characteristics of materials, detection techniques in the microwave range can be roughly categorized into three main classes: free-space approaches [15], [16], transmission-line approaches [17], [18] and resonant cavity approaches [19]. For the free-space technique, a MUT sample is placed between two directional antennas. Dielectric information is obtained by measuring the transmission or reflection coefficients. Nevertheless, large sample volume is often required, which accounts for its main disadvantage. In the transmission-line method, a material sample is inserted into a section of transmission line such as waveguide and strip-line. The resultant frequency response due to material filling contains the permittivity information. The drawback of this technique lies in the difficulty of sample preparation.

The resonant cavity method records the resonant response deviation before and after material filling into the cavity. Because of the high quality factor of a metallic cavity, very tiny perturbation can be distinguished, thus it is the most accurate technique among all these three methods. However, traditional cavity features a three dimensional structure, which is bulky and incompatible to planar circuits. Therefore, low-cost and planar sensing elements with good sensitivity are highly desirable in the microwave domain to characterize material with high accuracy. In the past few years, several new planar electro-magnetic configurations have been reported. The most representative ones are the split ring resonator (SRR) [20] and its complementary version (CSRR) [21], [22]. Taking SRR as an example, when the SRR is exposed to a MUT sample, the electrical field distribution can be altered. Based on the corresponding frequency responses, the permittivity information can be extracted.

Nevertheless, the excitation of SRR is somewhat difficult, and thus the sensitivity is reduced as a result. For the CSRR case, its ground is patterned and its integrity is therefore broken. These factors give rise to compatibility problems in many practical circuits, and thus limit the application aspects.

To measure the frequency response in an accurate manner, a vector network analyzer (VNA) is often required. Therefore, it is expensive and inconvenient in many circumstances. In order to reduce the system complexity and cost, it is of great importance to develop a low-cost and integrated permittivity sensor solution for future applications. In addition, the data readout must be sufficiently convenient and simple.

In this work, the compact microwave resonant cell (CMRC) is proposed as a microwave dielectric constant sensor, as its frequency performance changes when exposed to a MUT sample. Due to its planar configuration and dimensional compactness, it can be readily integrated into a phase locked loop (PLL) based frequency synthesizer. The MUT permittivity characterization is transformed to a simple task: voltage measurement. As a consequence, bulky and costly VNA is no longer needed, which greatly improves detection efficiency and reduces monetary expense.

The rest of this work is organized as follows: Section II introduces the concept and design guidelines of the proposed microwave sensor integrated with a VCO. Section III discusses the configuration of the whole sensing system as well as the material characterization procedure. In Section IV, the circuit realization and the measurement results are presented, followed by conclusion in Section V.

II. MICROWAVE SENSOR BASED ON CMRC

A. CMRC

The CMRC configuration, firstly proposed in 2000, is a popular electrical band-gap (EBG) structure with microstrip alike configuration. Due to its inherent band-stop characteristics and slow-wave effect, CMRC and its evolved versions have found numerous microwave applications, as reported in the literature [23]–[25]. Fig. 1 shows the typical structural diagram of a CMRC unit and its equivalent circuit in the form of lumped elements consisting of inductors and capacitors. As a typical frequency-selecting component, the resonant frequency f_{res} of a CMRC unit is roughly expressed as

$$f_{res} = \frac{1}{2\pi} \cdot \frac{1}{\sqrt{(4L_1/(\frac{1}{4C_0} + \frac{1}{2C_P}))}} \tag{1}$$

where L_1, C_0 and C_P are equivalent inductors and capacitors, as shown in Fig. 1(b). Note that the inductive parts are mainly produced by the longitudinal and transverse narrow lines, while the capacitances C_0 and C_P are generated by the mutual coupling between the metallic patterns and the coupling between the triangular patches and ground, respectively.

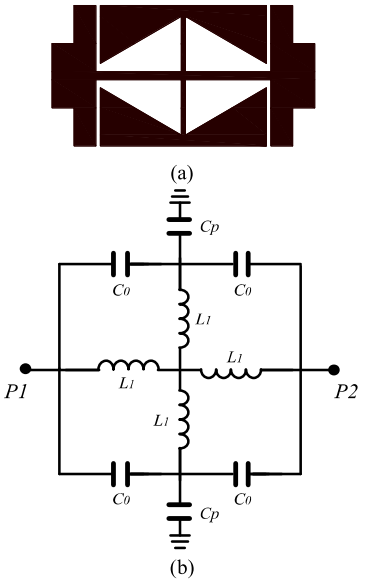

FIGURE 1. (a) Typical diagram of a CMRC unit. (b) *L-C* equivalent circuit of CMRC.

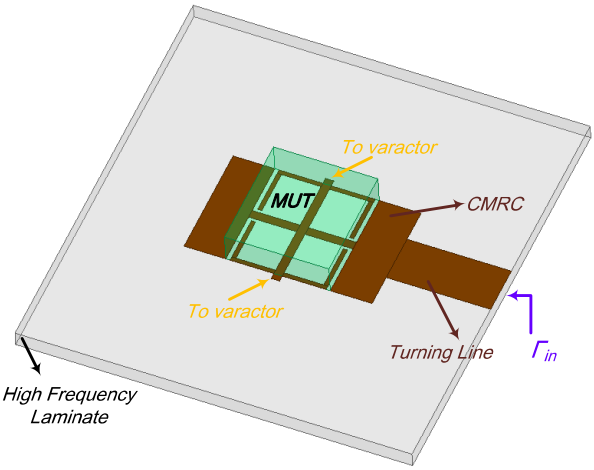

FIGURE 2. 3D illustration of the sensor configuration based on CMRC.

B. SENSING ELEMENT DESIGN

In this work, a microwave dielectric constant sensor is devised based on CMRC. As noted from (1), different capacitive or inductive elements can lead to distinct frequency responses. Therefore, it can be used as an effective sensing element under external perturbation by utilizing its frequency characteristics. Fig. 2 depicts the illustrative diagram of the proposed dielectric sensor. One end of CMRC is open circuited while the other end is connected with a section of transmission line, and a MUT sample cube is placed above it. Besides, two varactors are connected to the center taps, whose function will be discussed in the following section.

As is well known, the frequency-dependent material permittivity can be expressed in a complex form, $\varepsilon_r(\omega) = \varepsilon_r'(\omega) - j\varepsilon_r''(\omega)$, where $\varepsilon_r'(\omega)$ and $\varepsilon_r''(\omega)$ are the real and imaginary parts, respectively. The real part indicates the energy

storage within material, and the imaginary part is a measure of the material's loss. When a MUT sample is added, the field distribution of CMRC is perturbed. As $\varepsilon_r'(\omega)$ is generally larger than unity, which is corresponding to the dielectric permittivity of air, the electric fields would concentrate in the material disposed.

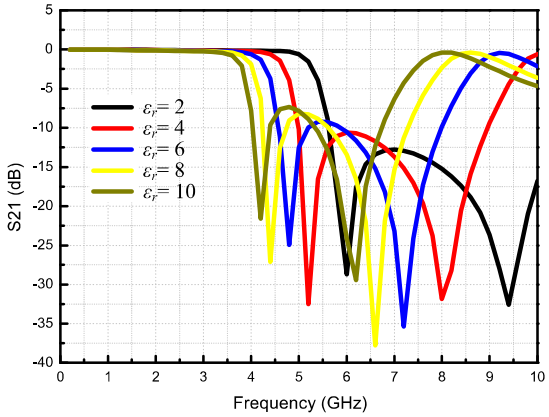

FIGURE 3. Simulated S21 curves of CMRC covered by a MUT cube with different ε_r values.

Alternatively speaking, when exposed to an exterior dielectric sample, the equivalent capacitance increases for CMRC. If the inductive parts are assumed intact, the resonant frequency decreases. Fig. 3 shows the simulated S21 curves of the CMRC unit covered by a MUT cube with $\varepsilon_r'(\omega)$ ranging from 2 to 10, with a step of 2. The MUT dimension is 15 mm × 6 mm × 4 mm, and $\varepsilon_r'(\omega)$ is assumed frequency invariable and the loss effect is neglected for analysis simplicity ($\varepsilon_r''(\omega) = 0$). Note that the resonant frequency (left S21 dip) is roughly dropped from 6 GHz for $\varepsilon_r'(\omega) = 2$ to 4.2 GHz for $\varepsilon_r'(\omega) = 10$. Therefore, it is intuitive that the material permittivity is closely related to the frequency response, and its detail information can be extracted if the frequency characteristics are properly exploited. In this context, CMRC is transformed into a feasible sensing element.

In addition, because of the planar and quasi-lumped structural feature, CMRC can be readily implanted into passive and active circuits as a single functional element. As a result, drawbacks of indirect signal excitation and defected ground encountered by SRR [20] and CSRR [21] are avoided. This greatly improves circuit performance and keeps the system compact in size and low in complexity.

C. VOLTAGE CONTROLLED OSCILLATOR DESIGN

In order to build an effective and low-cost sensing platform, the response of the sensitive detecting element must be read and expressed in a simple and precise manner. Many of previously published microwave sensing works mainly rely on scattering parameters (i.e., S-parameters) characterization. Although the S-parameters contain much valuable information, the S-parameter measurement requires an expensive and bulky vector signal analyzer (VNA), which inevitably increases the system cost and confines its application prospects. Herein, a synthesizer based microwave sensor with direct readout functionality is proposed to simplify system implementation.

As is well known, an oscillator is the key component of a frequency synthesizer. In the microwave frequency and above, oscillators can be roughly categorized into two different classes: feedback and reflective. The feedback type couples a portion of the output power into the input. Positive feedback is developed to generate oscillation by equalizing the overall phase of the loop to an integral multiple of 2π and having loop gain larger than unity. A resonator acting as the frequency selection element is generally embedded in the feedback loop, whose Q-factor largely determines the phase noise of the overall oscillator.

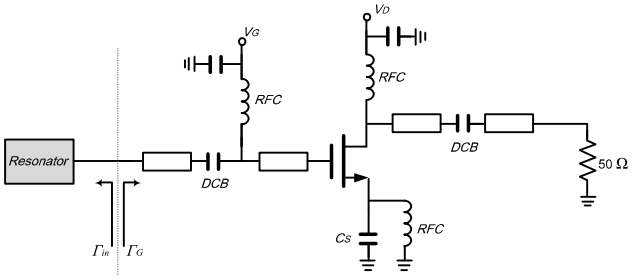

FIGURE 4. Typical schematic diagram of a reflective oscillator.

The reflective oscillator, on the other hand, reflects a part of the power back into the input to realize a negative impedance using a resonator. Observed from Fig. 3, the frequency notches appear for the S_{21} curves, which indicates a typical band-stop feature. As a consequence, the reflective scheme is herein chosen whereas the CMRC unit is applied as a reflecting resonator. Fig. 4 shows the simplified schematic diagram of the devised dielectric sensing apparatus. According to the oscillator design theory, the following requirements must be met to generate a stable oscillation,

$$|\Gamma_{in}| \times |\Gamma_G| > 1 \tag{2.a}$$

$$\angle\Gamma_{in} = -\angle\Gamma_G \pm 2K \cdot \pi \tag{2.b}$$

where Γ_{in} and Γ_G are the reflection coefficients seen into the transistor gate and the resonator respectively, and K is an arbitrary integral number. For practical circuit design, the absolute value of Γ_G is usually made larger than unity to meet the magnitude condition described by (2.a). A capacitor C_S is connected between the transistor source terminal and the ground to generate the negative resistance in this design. Specifically speaking, an ATF-34143 pHEMT from Avago Technologies is used as the active device. Provided with the transistor model, the stability analysis is conducted in Keysight ADS. Fig. 5 shows the simulated magnitude and phase curves as functions of the frequency for Γ_G with varied C_S. It is clearly observed that $|\Gamma_G| > 1$ is obtained in a wide frequency range for each C_S value. Therefore, the phase condition given by (2.b) remains as the determinant condition of the final oscillation frequency.

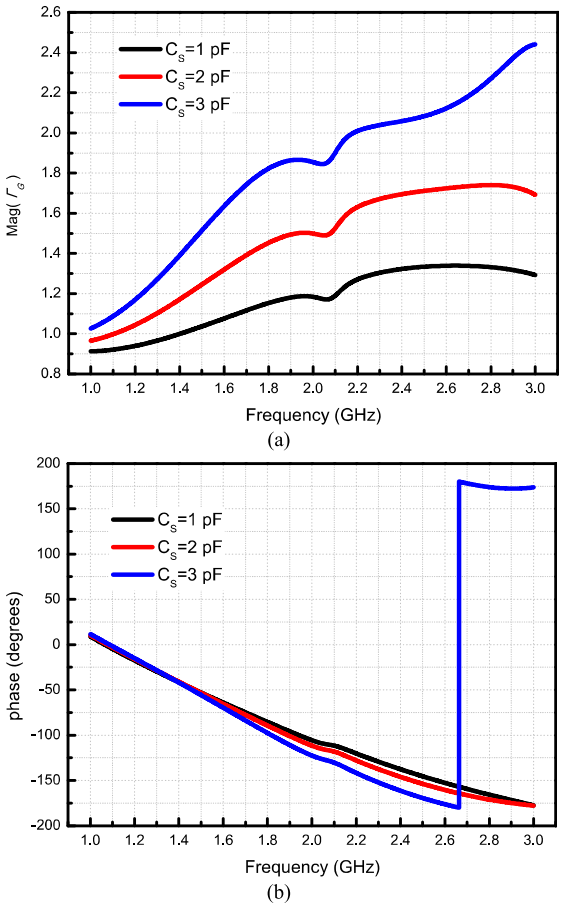

FIGURE 5. (a) Simulated magnitude of Γ_G versus frequency for different C_S values. (b) Simulated phase of Γ_G versus frequency for different C_S values.

According to the previous analysis, when CMRC is used as a resonator, the impedance changes if different MUT samples are loaded, and the resultant free-running frequency shifts accordingly. From the circuit design aspect, in order to finalize a complete frequency synthesizer, electrically tunable components should be applied to the resonator or active device. In this design, two reverse biased varactors are added to the center tap of the CMRC unit, as shown in Fig. 2. If loss and parasitic effects of varactor are neglected for simplicity, they are modeled as ideal capacitors whose actual capacitance are determined by the applied reverse voltage. In this scenario, the resonating frequency of the updated resonator loaded with MUT and varactors can be written as

$$f'_{res} = \frac{1}{2\pi} \cdot \frac{1}{\sqrt{(4L_1/(\frac{1}{4C_0} + \frac{1}{2C_P} + \frac{1}{C_{ext}})}}$$
$$C_{ext} = 1/\frac{1}{C(\varepsilon_r)} + \frac{1}{2C_V}) \quad (3)$$

where $C(\varepsilon_r)$ denotes the additional capacitance caused by the added MUT sample, whose value is proportional to its permittivity, and C_V stands for the capacitance of each varactor. Therefore, it is readily seen that the eventual frequency is jointly determined by interactions among the CMRC resonator exposed to MUT, the biased varactor and the active device.

III. SENSING PLATFORM USING FREQUENCY SYNTHESIZER

A. FRACTIONAL-N PLL BASED FREQUENCY SYNTHESIZER

From the aforementioned analysis, the resonator response variation due to MUT exposure can cause frequency shift of the microwave oscillator. Nevertheless, a bulky and expensive signal analyzer is still needed to accurately characterize this frequency change for a traditional solution. Therefore, a step forward is herein taken to realize a cost-effective sensor system. To be specific, a VCO based on CMRC is embedded into a fractional-*N* PLL.

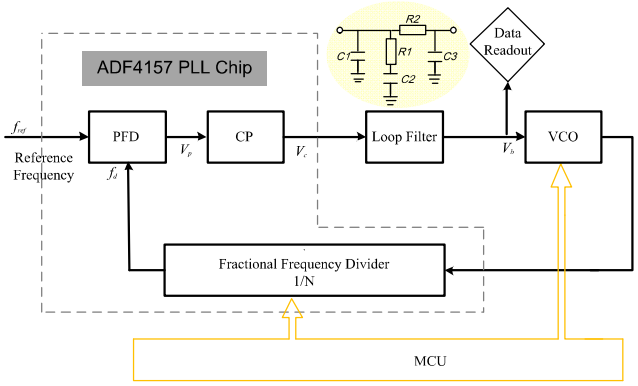

FIGURE 6. System diagram of the proposed sensor platform.

Fig. 6 shows the complete schematic diagram of the devised sensor platform. It consists of three main blocks: VCO, PLL, and microcontroller unit (MCU). The VCO is used to generate an oscillation signal whose frequency is sensitive to the MUT and affected by the varactor biasing voltage, as analyzed above. To establish a precise mapping relationship between the material permittivity value and the voltage applied to VCO, a PLL is introduced as a stabilizing element. The PLL apparatus contains a fractional frequency divider (FD), a phase frequency detector (PFD), a charge pump (CP) and a loop filter (LPF).

To miniaturize circuit size and accelerate circuit prototyping, an off-the-shelf frequency synthesizer is used, which integrates a programmable FD, PFD and CP in a single chip. The operation principle are roughly summarized as follows. An external crystal provides the PLL chip with a high-quality reference frequency f_{ref}, which is compared with the divided VCO output f_d in the internal PFD. The PFD generates a voltage V_p that is proportional to the phase difference between f_{ref} and f_d. The regulated voltage V_c after CP is then sent to a third-order loop filter (LPF), which is not included in the synthesizer chip. The configuration of the devised LPF is shown in the inset of Fig. 6. Moreover, it is worth noting that if a large capacitance tuning ratio of varactor and hence a large detection range of sensor are required, an active LPF

containing an operation amplifier (OPA) can be designed to increase voltage dynamics.

The filtered voltage V_b is finally used to regulate the varactors, which is alternatively named as the VCO controlling voltage. At this point, the resonator response is successfully mapped to a DC controlling voltage, which can be readily measured with a multi-meter or processed with a high resolution analog-to-digital converter (ADC). Consequently, the entire system complexity is reduce to a low level, as costly and troublesome frequency measurement is no longer necessary anymore. The MCU is introduced to program the frequency division ratio N and control the operation of the whole system.

B. SYSTEM SETUP AND DETECTION PROCEDURE

This subsection introduces the system setup and material characterization procedure of the built platform. Suppose the frequency of the standalone free-running oscillator with no material placed on CMRC and no voltage applied to varactors is f_0, whose value can be measured by a signal analyzer. The first step of the characterization process is embedding the proposed VCO to the PLL. That is, the VCO output is connected to the RF input of the PLL board, and the LPF regulated output voltage V_b, as shown in Fig. 6, is used to bias the varactors in the VCO.

The second step is to set an initial frequency division ratio N by writing proper values into the registers of the PLL chip by MCU. According to the operation principle of PLL based frequency synthesizer, the final output frequency f_{LCK} of the locked VCO can be expressed as

$$f_{LCK} = N \cdot f_{ref} \tag{4}$$

where N can be an integer or a fractional number. The f_{LCK} value is chosen to be identical with f_0. The locking status can be checked by simply investigating the VCO output frequency in a signal analyzer to see whether equation (4) holds. The bias voltage at this initialization point $V_{b,0}$ should be zero.

In the third step, the MUT sample is placed on top of the CMRC unit. Based on the previous analysis, the MUT material is going to change the VCO free-running oscillation frequency as the resonator equivalent capacitance is altered. However, due to the existence of PLL, the eventual oscillation frequency is pulled back to f_0 by modulating the bias voltage $V_{b,mut}$ automatically inside the frequency synthesizer.

From another observation aspect, this constant frequency characteristic is achieved because the sum of capacitances induced by the MUT sample and varactors is invariable. That is, the term C_{ext} is constant in equation (3). As a consequence, one can infer that a higher MUT permittivity results in a larger capacitance $C(\varepsilon_r)$, and thus a smaller compensated capacitance C_V is required from the varactors.

Fig. 7 depicts the capacitance values versus the reverse bias voltage of several varactors. As can be seen, the capacitances decrease exponentially when the reverse voltage increases. Therefore, it is readily to conceive that $V_{b,mut}$ increases when the MUT dielectric constant increases in the proposed system, and there exists a one-to-one correspondence between each other. In this context, the material permittivity value is successfully mapped to the VCO control voltage. The complicated task of oscillation frequency detection is then converted to the simple task of voltage measurement.

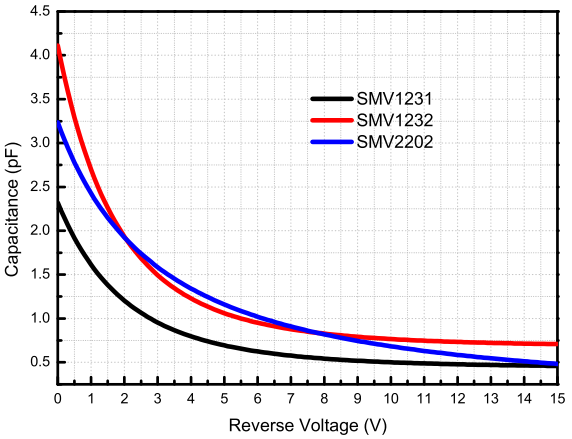

FIGURE 7. Typical varactor capacitances versus reverse voltage.

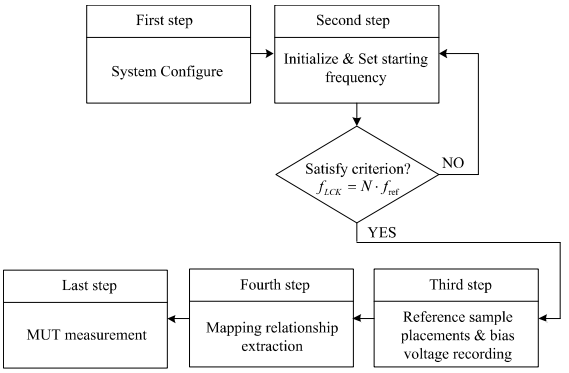

FIGURE 8. Flowchart of the whole permittivity detection procedure.

In the next step, a clear mapping is established by recording the corresponding V_b values of some calibrating materials with known values of permittivity. The voltage-permittivity relation can be obtained by curve fitting. Finally, the MUT permittivity is extracted with its corresponding bias voltage reading from the proposed synthesizer. Fig. 8 depicts the whole flow chart of the detection process of the proposed sensing platform.

IV. SYSTEM IMPLEMENTATION AND MEASUREMENT

Fig. 9 shows the photograph of the implemented microwave material sensor. The entire hardware includes two main parts: the VCO board and the PLL board. The VCO board is fabricated on Rogers 5780 laminate with permittivity of 2.33 and substrate height of 0.79 mm. Two silicon hyperabrupt junction varactors SMV1231-079LF from Skyworks Inc. are applied as the frequency tuning elements. Drain supplying and gate biasing voltages of the transistor are set to

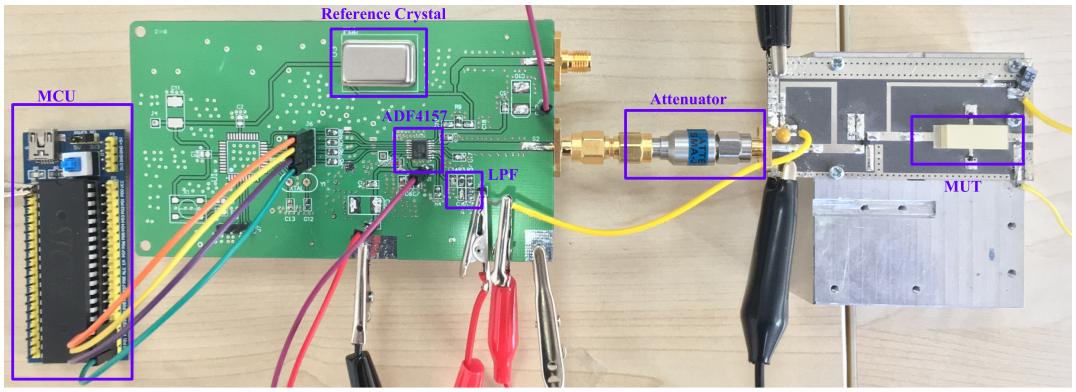

FIGURE 9. Photograph of the implemented sensor.

4 V and -0.6 V, respectively. The overall size of the RF board is 32 mm × 68 mm.

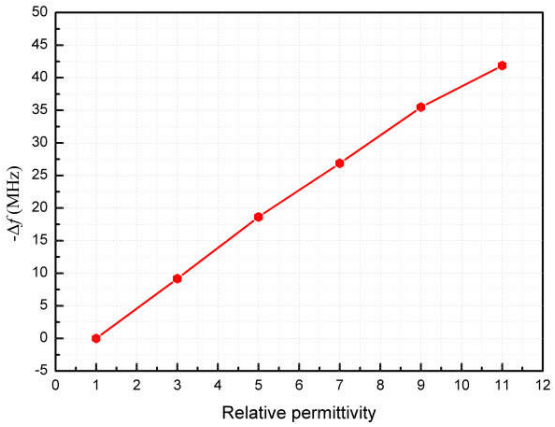

FIGURE 10. Simulated oscillation frequency shift versus MUT permittivity.

According to the preceding analysis, in the system startup and calibration stage, if no material is introduced to CMRC, $V_{b,0}$ is 0 V. The corresponding varactor capacitance is roughly 2.35 pF according to its datasheet. Fig. 10 depicts the simulated free-running oscillation frequency shift (in comparison with f_0) when the materials with different permittivity values are applied. It is readily noted that the oscillation frequency reduces when the MUT permittivity increases. This is because the material induced capacitance increases. The MUT cube dimension is 15 mm × 6 mm × 4 mm in length, width and height. It is worth noting that the varactor biasing voltages are kept zero in all simulations. The CMRC performance is simulated in Ansys HFSS and imported into ADS for co-simulation.

The PLL board, on the other hand, is fabricated on the low-cost FR4 laminate. Off-the-shelf components and chips are chosen to simplify circuit implementation. To be specific, the integrated synthesizer chip is ADF4157, which has a 25-bit fixed modulus, allowing subhertz frequency resolution. Hence, very tiny permittivity difference can be distinguished. The system configuration and parameter setup are conducted in the ADIsimPLL simulation tool.

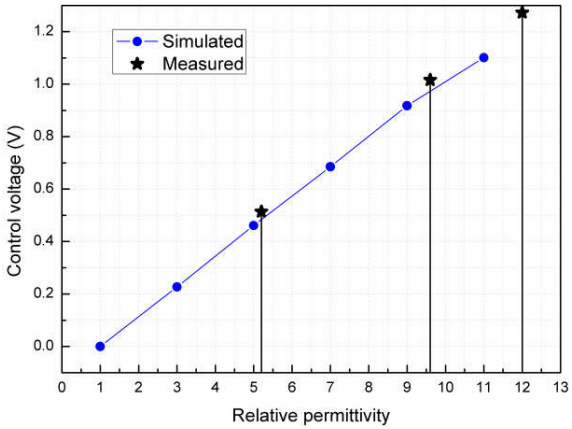

FIGURE 11. Measured and simulated bias voltage value versus material dielectric constant.

A three-order passive LPF is realized using discrete SMD resistors and capacitors. The exact values of R_1, R_2, C_1, C_2, and C_3, as shown in Fig. 6, are 1.5 kΩ, 2.9 kΩ, 240 pF, 3.2 nF and 100 pF respectively. Available practical components are chosen with values close to simulated ones. The corresponding loop bandwidth is about 20 kHz.

The VCO output is connected to the RF input terminal of the PLL board, with a 10-dB attenuator placed in-between. This is because the VCO output power is roughly 10 dBm and the maximum sustainable input power of the PLL chip is 0 dBm. For particular, the PFD reference frequency is 12 MHz, provided by the external crystal. The locked frequency is set as $f_{LK} = 1.24042$ GHz, therefore the frequency division ratio N is 103.368 according to (4). The values of inherent registers are written by MUT into the PLL chip.

In order to verify the effectiveness of the proposed system, three material cubes with known permittivity values of 5.2, 9.6 and 12 are tested sequentially, and their corresponding bias voltages are recorded as 0.514 V, 1.016 V, and 1.272 V using Keysight 34461A digital multi-meter with 1 mV resolution. The samples are carefully polished to have the same dimension as that is used in simulation. It is worth mentioning that the loss tangents of the tested materials are all in the order of 10^{-3} in the frequency band, therefore the effect of dielectric loss is neglected. Fig. 11 compares the bias voltage

profile versus the material permittivity from both simulation and measurement. It is readily seen that the control voltage has positive correlation with the MUT permittivity. The fitted mathematical relationship between the simulated bias voltage and dielectric constant is extracted as $V_{b,mut} = -0.12779 + 0.12346 \times \varepsilon_r - 0.0099 \times \varepsilon_r^2$. The shown discrepancy between the simulated and measured results are attributed to several factors such as device modeling inaccuracy, EM simulation uncertainty, fabrication tolerance, etc. However, the exact relationship between the MUT sample permittivity and the recorded DC voltage can be determined with sufficient accuracy if large number of samples with known properties are used for calibrating. Once the correspondence between the control voltage and the permittivity is established, the dielectric constant of unknown MUT can be readily extracted. With this mapping relationship in hand, the permittivity of unknown MUT is simply obtained by directly measuring the VCO biasing voltage.

V. CONCLUSION

In this work, a novel dielectric constant sensor was proposed using the microwave technique. The CMRC structure has been applied as the sensing element, which is high in sensitivity, compact in size and compatible to the planar circuits. By virtue of a frequency synthesizer, the material permittivity can be detected precisely by simply measuring the bias voltage of the microwave VCO. Therefore, the detection speed and sensitivity have been greatly improved. In the meantime, the system complexity and realization cost were largely reduced.

REFERENCES

[1] S. Trabelsi and S. O. Nelson, "Microwave sensing of quality attributes of agricultural and food products," *IEEE Instrum. Meas. Mag.*, vol. 19, no. 1, pp. 36–41, Feb. 2016.
[2] S. O. Nelson, W.-C. Guo, S. Trabelsi, and S. J. Kays, "Dielectric spectroscopy of watermelons for quality sensing," *Meas. Sci. Technol.*, vol. 18, no. 7, pp. 1887–1892, Jul. 2007.
[3] H.-W. Wu, "Label-free and antibody-free wideband microwave biosensor for identifying the cancer cells," *IEEE Trans. Microw. Theory Techn.*, vol. 64, no. 3, pp. 982–990, Mar. 2016.
[4] C. Dalmay, A. Pothier, P. Blondy, F. Lalloue, and M.-O. Jauberteau, "Label free biosensors for human cell characterization using radio and microwave frequencies," in *IEEE MTT-S Int. Microw. Symp. Dig.*, Jun. 2008, pp. 911–914.
[5] M. Hofmann, G. Fischer, R. Weigel, and D. Kissinger, "Microwave-based noninvasive concentration measurements for biomedical applications," *IEEE Trans. Microw. Theory Techn.*, vol. 61, no. 5, pp. 2195–2204, May 2013.
[6] K. Entesari, A. A. Helmy, and M. M.-Bajestan, "Integrated systems for biomedical applications: Silicon-based RFmicrowave dielectric spectroscopy and sensing," *IEEE Microw. Mag.*, vol. 18, no. 5, pp. 57–72, Aug. 2017.
[7] H. Choi *et al.*, "Design and *in vitro* interference test of microwave noninvasive blood glucose monitoring sensor," *IEEE Trans. Microw. Theory Techn.*, vol. 63, no. 10, pp. 3016–3025, Oct. 2015.
[8] X. Xiao and Q. Li, "A noninvasive measurement of blood glucose concentration by UWB microwave spectrum," *IEEE Antennas Wireless Propag. Lett.*, vol. 16, pp. 1040–1043, 2017.
[9] T. R. Jones, M. H. Zarifi, and M. Daneshmand, "Miniaturized quarter-mode substrate integrated cavity resonators for humidity sensing," *IEEE Microw. Wireless. Compon. Lett.*, vol. 27, no. 7, pp. 612–614, Jul. 2017.
[10] H. El Matbouly, N. Boubekeur, and F. Domingue, "Passive microwave substrate integrated cavity resonator for humidity sensing," *IEEE Trans. Microw. Theory Techn.*, vol. 63, no. 12, pp. 4150–4156, Dec. 2015.
[11] G. Barochi, J. Rossignol, and M. Bouvet, "Development of microwave gas sensors," *Sens. Actuator B, Chem.*, vol. 157, pp. 374–379, Oct. 2011.
[12] V. Sekar, W. J. Torke, S. Palermo, and K. Entesari, "A self-sustained microwave system for dielectric-constant measurement of lossy organic liquids," *IEEE Trans. Microw. Theory Techn.*, vol. 60, no. 5, pp. 1444–1455, May 2012.
[13] A. Ebrahimi, W. Withayachumnankul, S. Al-Sarawi, and D. Abbott, "High-sensitivity metamaterial-inspired sensor for microfluidic dielectric characterization," *IEEE Sensors J.*, vol. 14, no. 5, pp. 1345–1351, May 2014.
[14] M. H. Zarifi, M. Rahimi, M. Daneshmand, and T. Thundat, "Microwave ring resonator-based non-contact interface sensor for oil sands applications," *Sens. Actuators B, Chem.*, vol. 224, pp. 632–639, Mar. 2016.
[15] M. Nakhkash, Y. Huang, W. Al-Nuaimy, and M. T. C. Fang, "An improved calibration technique for free-space measurement of complex permittivity," *IEEE Trans. Geosci. Remote Sens.*, vol. 39, no. 2, pp. 453–455, Feb. 2001.
[16] D. K. Ghodgaonkar, V. V. Varadan, and V. K. Varadan, "Free-space measurement of complex permittivity and complex permeability of magnetic materials at microwave frequencies," *IEEE Trans. Instrum. Meas.*, vol. 39, no. 2, pp. 387–394, Apr. 1990.
[17] P. M. Narayanan, "Microstrip transmission line method for broadband permittivity measurement of dielectric substrates," *IEEE Trans. Microw. Theory Techn.*, vol. 62, no. 11, pp. 2784–2790, Nov. 2014.
[18] M. J. Akhtar, L. E. Feher, and M. Thumm, "A waveguide-based two-step approach for measuring complex permittivity tensor of uniaxial composite materials," *IEEE Trans. Microw. Theory Techn.*, vol. 54, no. 5, pp. 2011–2022, May 2006.
[19] A. W. Kraszewski, S. O. Nelson, and T.-S. You, "Use of a microwave cavity for sensing dielectric properties of arbitrarily shaped biological objects," *IEEE Trans. Microw. Theory Techn.*, vol. 38, no. 7, pp. 858–863, Jul. 1990.
[20] W. Withayachumnankul, K. Jaruwongrungsee, A. Tuantranont, C. Fumeaux, and D. Abbott, "Metamaterial-based microfluidic sensor for dielectric characterization," *Sens. Actuators A, Phys.*, vol. 189, pp. 233–237, Jan. 2013.
[21] M. S. Boybay and O. M. Ramahi, "Material characterization using complementary split-ring resonators," *IEEE Trans. Instrum. Meas.*, vol. 61, no. 11, pp. 3039–3046, Nov. 2012.
[22] M. A. H. Ansari, A. K. Jha, and M. J. Akhtar, "Design and application of the CSRR-based planar sensor for noninvasive measurement of complex permittivity," *IEEE Sensors J.*, vol. 15, no. 12, pp. 7181–7189, Dec. 2015.
[23] S. Chen and Q. Xue, "A class-F power amplifier with CMRC," *IEEE Microw. Wireless Compon. Lett.*, vol. 21, no. 1, pp. 31–33, Jan. 2011.
[24] Q. Xue, K. M. Shum, and C. H. Chan, "Low conversion-loss fourth subharmonic mixers incorporating CMRC for millimeter-wave applications," *IEEE Trans. Microw. Theory Techn.*, vol. 51, no. 5, pp. 1449–1454, May 2003.
[25] K. M. Shum, Q. Xue, and C. H. Chan, "A novel microstrip ring hybrid incorporating a PBG cell," *IEEE Microw. Wireless Compon. Lett.*, vol. 11, no. 6, pp. 258–260, Jun. 2001.

SHICHANG CHEN (S'09–M'14) received the B.S. degree in electronic engineering from the Nanjing University of Science and Technology in 2009 and the Ph.D. degree in electronic engineering from the City University of Hong Kong in 2013.

From 2013 to 2014, he was with the City University of Hong Kong as a Post-Doctoral Fellow. He is currently with Hangzhou Dianzi University as an Associate Professor. His research interest focuses on high-efficiency power amplifier, integrated circuits, and sensors.

MENGCHU GUO received the B.Eng. degree from Henan Polytechnic University, Jiaozuo, China, in 2016. He is currently pursuing the M.S. degree with a focus on microwave sensors in Hangzhou Dianzi University.

KUIWEN XU received the B.E. degree from Hangzhou Dianzi University in 2009 and the Ph.D. degree from Zhejiang University, Hangzhou, China in 2014. He was a Visiting Ph.D. Student with the National University of Singapore, Singapore, from 2012 to 2013. From 2014 to 2015, he was with Huawei Technologies Co., Ltd. He is currently an Associate Professor with Hangzhou Dianzi University. His research interests include antenna design, microwave measurement, and electromagnetic inverse problems.

PENG ZHAO (S'12–M'16) received the B.Eng. and M.Phil. degrees from the Electronic Engineering Department, Zhejiang University, China, in 2006 and 2008, respectively, and the Ph.D. degree in electronic engineering from the City University of Hong Kong, China, in 2014. He is currently a Faculty Member with the Key Laboratory of RF Circuits and Systems, Ministry of Education, Microelectronics CAD Center, Hangzhou Dianzi University, Hangzhou, China. He is also with the State Key Laboratory of Millimeter Waves, Southeast University, Nanjing, China. His research interests include microwave devices and computational electromagnetics.

LINXI DONG received the Ph.D. degree in the major of microelectronics and solid electronics from Zhejiang University, Hangzhou, China, in 2004. He is currently a Professor with Hangzhou Dianzi University, where he is involved in the design and fabrication of MEMS sensors, resonators, wireless sensor network, and integrated circuit.

GAOFENG WANG (S'93–M'95–SM'01) received the Ph.D. degree in electrical engineering from the University of Wisconsin–Milwaukee, Milwaukee, WI, USA, in 1993, and the Ph.D. degree in scientific computing from Stanford University, Stanford, CA, USA, in 2001.

He was a Scientist with Tanner Research Inc., Pasadena, CA, USA, from 1993 to 1996. He was a Principal Researcher and a Development Engineer with Synopsys Inc., Mountain View, CA, USA, from 1996 to 2001. In 1999, he served as a Consultant with Bell Laboratories (Nokia Bell Labs), Murray Hill, NJ, USA. He was the Chief Technology Officer (CTO) of Intpax, Inc., San Jose, CA, USA, from 2001 to 2003. He was the CTO of Siargo Inc., Santa Clara, CA, USA, from 2004 to 2010. He was a Professor and the Head with the CJ Huang Information Technology Research Institute, Wuhan University, Wuhan, China, from 2004 to 2013. He was the Chief Scientist with Lorentz Solution, Inc., Santa Clara, CA, USA, from 2010 to 2013. He is currently a Distinguished Professor with Hangzhou Dianzi University, Hangzhou. He has authored over 160 journal articles and holds 22 patents. His current research interests include integrated circuit and microelectromechanical system design and simulation, computational electromagnetics, electronic design automation, and wavelet applications in engineering.